A mesh deformation based approach for digital facial reconstruction

Maya de Buhan, Chiara Nardoni

A mesh deformation based approach for digital facial reconstruction

Maya de Buhan[1*]

[1] *CNRS, UMR 8145, MAP5, Université Paris Descartes, Sorbonne Paris Cité, France*

Chiara Nardoni[2†]

[2] *Sorbonne Universités, UPMC Univ Paris 06, Institut des Sciences du Calcul et des Données, F-75005, Paris, France*

November 23, 2016

Abstract

This article presents a numerical method for facial reconstruction. The problem is the following: if I only have a dry skull, can I reconstruct a virtual face that would enhance the identification of the subject? Our approach combines classical features as the use of a skulls/faces database to learn the relations between the two items and more original aspects: (i) we use an original shape matching method to link the unknown skull to the database templates; (ii) the final face is seen as an elastic 3d mask which is adapted onto the unknown skull. Using our method the skull is considered as a whole surface - represented by a surface triangulation - and not restricted to some anatomical landmarks, allowing a dense description of the skull/face relationship. In particular, our approach is fully-automated. We present some preliminary results to show its efficiency.

Keywords: facial reconstruction, shape matching, elasticity, soft tissue deformation, finite elements.

1 Introduction

Facial reconstruction aims at recovering the facial appearance of an individual from the sole datum of the underlying skull. The facial reconstruction problem arises in various application fields like forensics, anthropology, archeology or history. In forensic science, facial reconstruction comes in the process of identification of deceased people.When all the usual methods of identification have failed and the skeletal remain is the sole datum available for leading to a positive identification, facial reconstruction might be considered as an enhancing tool for 'recognition', producing a short list of candidates from which the individual may be identified by other endorsed methods of identification [42]. In archeological investigations, facial reconstruction is employed with the purpose of identifying skeletal remains of famous people from the past. The creation of the face from the skull is a procedure of *approximation*: from the observation of the cranium, one will not be able to recover a big amount of face features (eyes, hair, lips, ears). Moreover the facial likeness of a single individual changes considerably depending on factors like nutrition or aging. This flexibility may not be fully reflected on the subjacent skull. Any facial reconstruction tool is expected to account somewhere for the uncertainty related to the *ill-posedness* of the problem, no matter which method is employed (artistic, parametric, statistic, mechanical, etc.). From a mathematical point of view, this issue

*e-mail: maya.de-buhan@parisdescartes.fr

†e-mail: chiara.nardoni@upmc.fr

leads to at least two important difficulties: on the one hand, it raises the question of how to correctly characterize the solution, which might be a continuum spectrum of all faces 'consistent' with a given skull rather than a single exemplar; on the other hand, it poses the problem of how to rigorously assess the accuracy of the result. Despite the intrinsic difficulty of the problem, the media are full of facial images that have been constructed on the basis of a single given skull. A fascinating survey of such cases can be found in the book [33]. The work presented in this paper is part of the ongoing multi-disciplinary project FaciLe [1], grouping together maxillo-facial surgeons, anthropologists, computer scientists and mathematicians from Sorbonne Universités.

The traditional facial reconstruction methods are based on manual procedures, producing 2d portraits or 3d sculptures. These methods basically consist of three common steps: (i) equip (a replica of) the raw skull with a sparse set of anatomical landmarks; (ii) apply an average soft tissue thickness to each skull landmark in order to estimate a corresponding landmark on the face; (iii) draw up or sculpt a face fitting the estimated landmarks. Most practitioners add a face muscles model in order to enrich the anatomical accuracy of the reconstruction, leading to the so called Manchester method [42]. The results obtained from forensic art are often quite plausible, as the medical artists may take anatomical, historical, archaeological or other type of expertise into account, giving the observer a feeling of coherence. However, the final result of a manual reconstruction depends strongly on the subjectivity of the artist. Additionally, one single reconstruction requires several days of work of a well-experienced forensic artist, making impracticable the realization of multiple instances and feature variations. In order to alleviate these difficulties, several computer graphic softwares have been developed with the purpose of assisting the facial reconstruction. These animation softwares use the same methodology as manual methods, allowing the expert to tune some modeling parameters and combine the human expertise with the flexibility of the software [30]. However, this approach does not eliminate the attribute of subjectivity in the reconstruction. During the last 30 years an important deal of work has been devoted to the conception of objective fully-automated methods. The common pipeline of modern facial reconstruction softwares is described in [11]. First, an expert examines the unknown skull in order to determine anthropological parameters like age, gender and ethnicity. Then a virtual replica of the dry skull is produced and represented according to the modeling parameters. A craniofacial template encoding face, skull and soft tissue information is derived from a head database. Then an admissible geometric transformation drives the adaptation of the craniofacial template onto the unknown skull, according to the 'proximity' between the skulls. As a result the template face is deformed onto the 'predicted' face associated with the unknown skull, linking together both information coming from the database and the examination of the unknown skull. Finally a skin texture and hairiness are added to the reconstructed face.

Our approach combines classical features -as the use of a head database or the anthropological expertise for classifying the unknown skull - with mathematical and computational skills as partial differential equations (PDE), numerical analysis, 3d geometric modeling. The contribution of this work is threefold. First, we introduce a method for generating a closed surface mesh model of the skull template. Our method rely on an original PDE based mesh evolution technique. A template shape is iteratively deformed producing a sequence of shapes which get 'closer and closer' (in a metric sense) to the source skull. Second, we present the elastic shape matching method we first introduced in [7]. This technique is used to link skulls (faces, respectively) with each other and learn about their similarities. This procedure is the heart of our reconstruction method and the most original part. In particular it allows the method to be fully-automated by removing the need of landmarks. Third, we combine our shape matching tool with soft tissue deformation techniques from computational surgery for transporting the skull/face templates onto the unknown skull. The common denominator of the three parts is the use of elasticity equations for driving the shape (and corresponding mesh) deformation. Using only geometric distance based criterion may impose an

[1] http://www.sorbonne-universites.fr/actions/recherche/chaires-thematiques/facile.html

important stretching in the deforming shape, making the motion of its vertices impossible to achieve without invalidating the mesh. Owing to the mechanical features of elastic displacements (notably their 'rigidity') and to the regularizing effect of elastic equations, the desired transformation is expected to be easier to achieve in numerical practice, resulting in valid mesh configurations and limiting troubles due to mesh tangling.

The paper is organized as follows: Section 2 deals with the acquisition and the construction of the database; Section 3 describes the representation of the skull templates; Section 4 presents our method for matching skull and face templates; Section 5 describes the process of reconstruction of the unknown face and in Section 6 we present one facial reconstruction to prove the efficiency of our approach. Figure 1 summarizes the different steps of the procedure.

2 Data acquisition

All current numerical facial reconstruction methods repose on the *a priori* information contained in a database of coupled skull and face templates. The acquisition of both skull and face is accomplished by head CT scans of living subjects, allowing a good visualization of hard tissues. Standard segmentation tools and 3d reconstruction algorithms lead to the definition of dense surfaces of both skull and face from CT data. Unfortunately the invasiveness of this technique causes serious legal and ethical problems, making troubling the constitution of a large database of healthy subjects. Due to this difficulty, several studies have proposed to exploit the relationship between soft and hard tissues by means of average soft tissue thickness measurements [39, 24, 20].

Soft tissue depth tables are usually used in combination with a large database of face templates [11]. Facial templates can be acquired by non-invasive techniques such as stereophotogrammetry [22] making the constitution of a large database painless and easy. However, despite the acquisition of dense surface templates for describing the outer face, the average values of soft tissue thickness are systematically measured on a sparse set (< 53) of (manually positioned) anatomical landmarks. Since the manual measurement is time consuming and requires expertise in correctly identifying the landmarks, it is actually infeasible to extend these measurements to a dense distribution of points [11]. See [27] for a discussion about the use of sparse soft tissue measurements for facial reconstruction purposes. Several authors have claimed the importance of using a dense representation of the soft tissue information, for example by describing the intra-subject correlation in terms of the volume between the two boundary surfaces representing the face and the underlying skull [34, 35]. The results presented in this study are based on a collection of 26 head CT scans of female healthy subjects aged between 20 and 40 years. The BMI index of the subjects is known but up to now not included in our study. The CT images used have been provided by the Statistical Facial Reconstruction project of Paris Descartes University [38]. The 3d reconstruction from tomographic data described in this section combined with an original wrapping method (see Section 3) allow us to define closed surface models of both face and skull.

2.1 Image segmentation

The data segmentation consists in identifying the bone and soft tissues on the stacked 2d gray-level images. This procedure has been carried out in a semi-automated way with the help of the software Amira [37]. First, the CT slices are automatically pre-segmented using a multi-threshold technique. This step consists in partitioning the original images into subdomains which boundaries are identified by given intensity values. The bone and soft tissues threshold values we used are described in [38]. From the pre-segmentation step we obtain two sets of binary images, respectively for bone and soft tissues. By stacking these slices we can essentially detect the 3d structures. However the intensity-based segmentation is not enough to ensure a correct separation of the tissues of interest, due to the presence of noise on the data and artifacts occurred during the acquisition

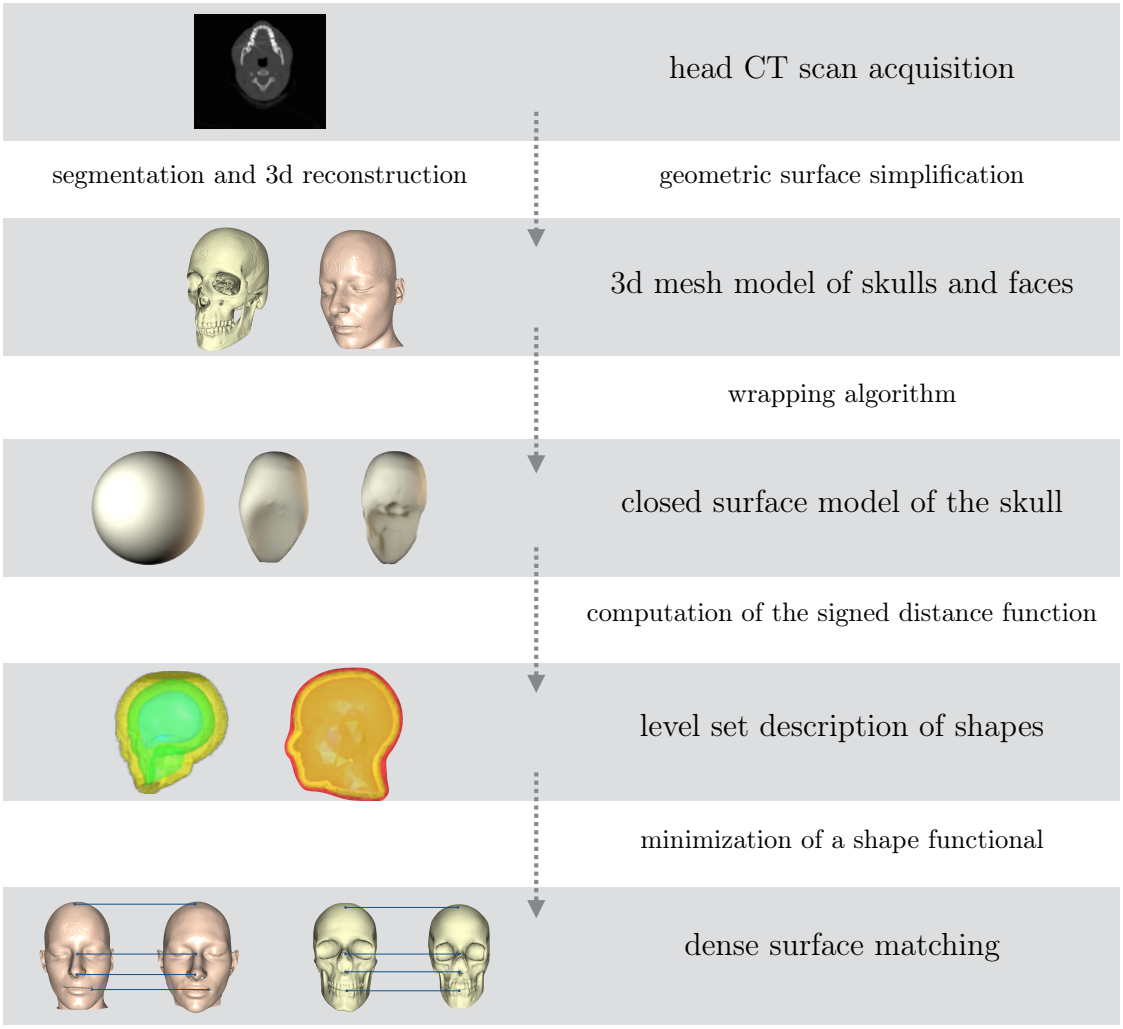

Figure 1 – From CT scans to densely matched surface templates (see Sections 2,3,4).

process. The binary images are then cleaned by removing the so-called islands (very small structures which contours are defined by only a few pixels). These structures can be external to the tissues of interest (noise added during the acquisition process) or very thin internal structures (small bones inside the cranium). This action helps in denoising the images. Moreover in most of the subjects we observed large artefacts on the images due to dental filling. These defects need to be manually removed on each affected slice (see Figure 2). After the correct identification of the subdomains of interest, we proceed in separating the cranium from the vertebral column. This operation is also done manually by labeling the cranium and the vertebral column on the 2d slices. See Figure 3. Finally the vertebral column is excluded from the bone label because it has no influence on the facial appearance of the individual.

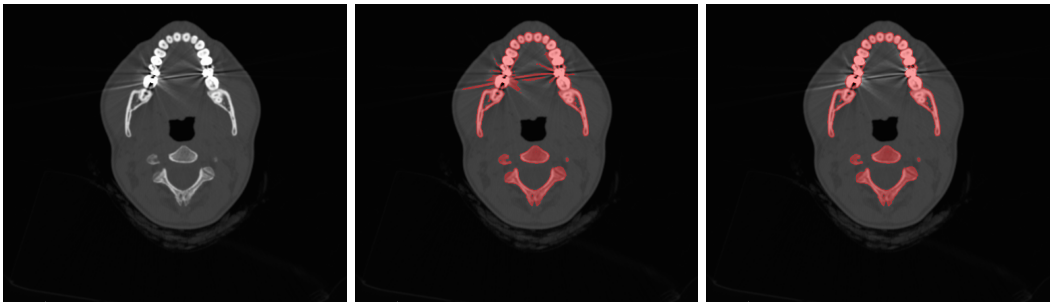

Figure 2 – Left: reference gray-level image. Middle: pre-segmentation of the bone using a threshold technique (red). Right: segmentation of the bone after denoising and artifacts removal (red).

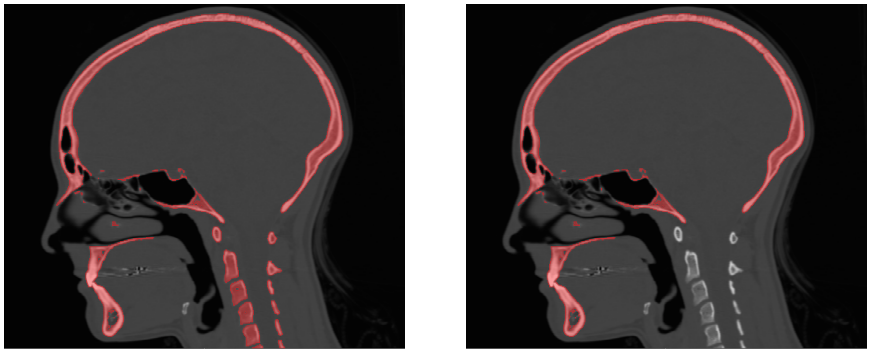

Figure 3 – Segmentation of the bone (red) (a) including vertebral column; (b) after removing vertebral column.

2.2 Geometric mesh processing

From the segmented 2d slices we generate 3d mesh models of the skull and the face by a marching cube algorithm [37]. These initial meshes contain, in general, a prohibitive number of elements which are redundant and oversampled to correctly describe the geometry of the model. These dense meshes are simplified thanks to the surface remeshing tool *mmgs* [15] by a local modification approach. The remeshing procedure aims at providing (i) a correct and accurate geometric approximation of the underlying 3d model (geometric mesh) and (ii) a computational mesh of high quality elements suitable for finite elements simulations (computational mesh). To ensure vicinity between the

original and the remeshed triangulations, the remesher controls the discrete Hausdorff distance between the two sets of triangles. For this study we kept this quantity smaller than a prescribed tolerance of 0.1% of the bounding box size. The element size of the simplified mesh is locally adapted to the surface curvatures, ensuring a correct approximation of the surface geometry. See [15] for a detailed description of the remeshing features and [18] for a discussion about the generation of computational meshes from discrete anatomical data. As illustrated in Figures 4 and 5, this procedure also removes the 'staircases' artefacts due to the spatial discretization and connectivity. Note that the meshes obtained by segmentation, even after geometric simplification, may often show intersecting faces, resulting in an invalid configuration. Using an implicit description of shapes (see Section 4), our approach generates valid computational meshes from invalid data.

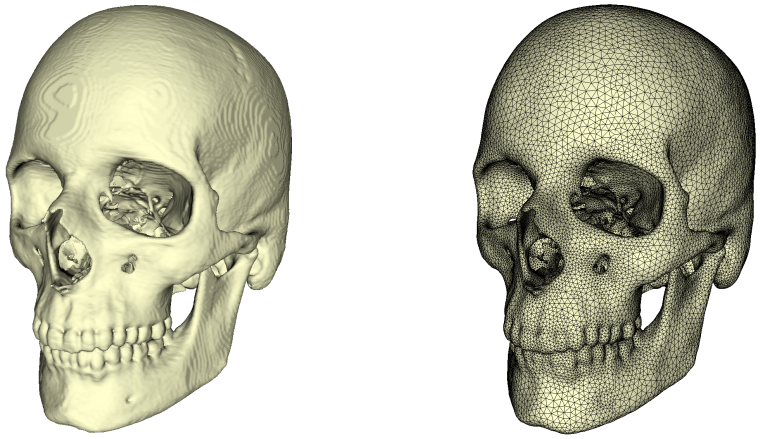

Figure 4 – Left: 3d mesh of the skull after segmentation (2179332 triangles). Right: 3d mesh of the skull after geometric remeshing (156301 triangles).

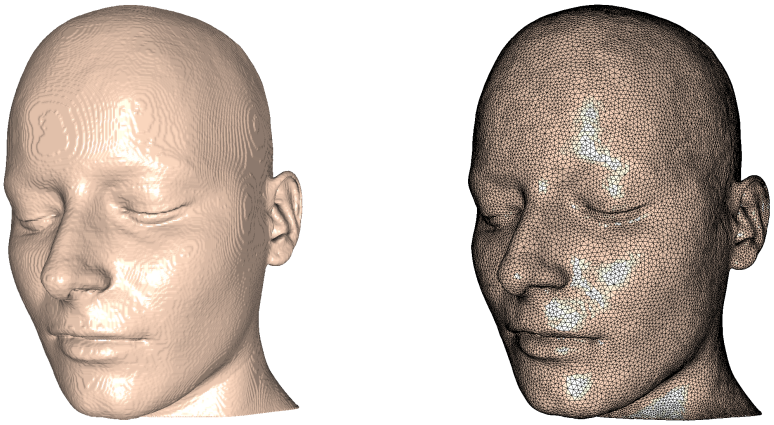

Figure 5 – Left: 3d mesh of the face after segmentation (1286542 triangles). Right: 3d mesh of the face after geometric remeshing (90949 triangles).

3 Generation of surface model of the skull

The human skull is characterized by a quite complex structure, showing small details which are difficult to acquire and to handle numerically. Due to these difficulties, several authors opt for describing the skull through underlying anatomical or geometrical substructures. The most popular choice lead to the definition of a sparse set of anatomical landmarks, eventually coupled with a dense representation of the skull [12]. Some authors use automatically detected continuous crest-lines [35]. The process of matching skull templates is then driven by the outlined feature structures, by requiring their best alignement.

The purpose of this section is to characterize the skull template in terms of a 3d bounded domain, known by a closed triangular mesh of its boundary. This issue is related to the more general problem of surface reconstruction from sample points, volumetric or CT data, as well as to the one of topology simplification for geometric processing and mathematical modeling. Surface reconstruction methods have been extensively investigated in the context of interface evolution via level set methods (see [13] and references therein) or via deformable surfaces [16, 29]. Our specific task, already evoked in [25, 39], is to define a closed surface model of the skull from tomographic data. In order to achieve this goal we propose an original wrapping algorithm based on mesh deformation techniques. First, we generate a (possibly invalid) source triangulation of the skull geometry by standard segmentation and 3d reconstruction tools (see Section 2). Then, a closed surface mesh model is iteratively deformed producing a sequence of surfaces (and corresponding meshes) which are 'closer and closer' to the source triangulation, in the sense of the Hausdorff distance. Since the shape topology is kept unchanged during deformation, the algorithm presented in this section generates a closed triangulation wrapping the skull. The generated triangulation partitions the ambient space in two subregions defining unambiguously an interior (resp. exterior) volume. This step is of crucial importance for matching shapes among the head database (see Section 4).

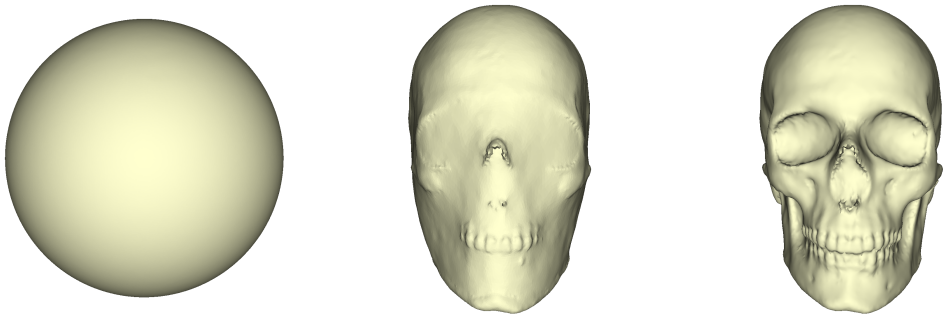

Figure 6 – Left: template shape Ω_0. Middle: advecting shape Ω_{10}. Right: finale shape Ω_{35}.

3.1 Presentation of the method

Let $\Omega_0 \subset \mathbb{R}^3$ be the template shape, analytically defined as the annular:

$$\Omega_0 = \{x \in \mathbb{R}^3 : r < |x| < R\} \quad r, R \in \mathbb{R}^+,$$

and let us introduce its internal boundary:

$$\Gamma_0 = \{x \in \mathbb{R}^3 : |x| = r\}.$$

Suppose that Ω_0 encircles $\mathcal{T}_S$ and assume that Γ_0 and $\mathcal{T}_S$ share a subset ω. The template shape is filled with a linear elastic material whose deformation is driven by the elasticity equations.

Elasticity equations *The displacement field of a shape Ω clamped at a part Γ^D of its boundary Γ and deflated under the effect of internal pressure $p \in H^{-1/2}(\Gamma^N)$ on $\Gamma^N = \Gamma \setminus \Gamma^D$ is achieved as the unique solution $u \in H^1_{\Gamma^D}(\Omega)^3 := \{w \in H^1(\Omega)^3, w = 0 \text{ on } \Gamma^D\}$ of the following variational problem:*

$$\int_\Omega \sigma(u) : \varepsilon(v)\, dx = \int_{\Gamma_N} pv \cdot n\, ds, \quad \forall v \in H^1_{\Gamma_D}(\Omega)^3. \tag{3.1}$$

where the stress tensor σ follows the Hooke's law:

$$\sigma(u) = 2\mu\varepsilon(u) + \lambda\ tr(\varepsilon(u))I,$$

with λ, μ the Lamé coefficients and $\varepsilon(u) = \frac{1}{2}(\nabla u + \nabla u^T)$ the linearized strain tensor.

Hence, starting from Ω_0, clamped at $\Gamma_0^D = \omega$ and deflated on $\Gamma_0^N = \Gamma_0 \setminus \Gamma_0^D$, we produce a sequence of shapes Ω_k, according to:

$$\Omega_{k+1} = (I + v_k)(\Omega_k), \tag{3.2}$$

where each displacement field v_k is defined from the solution u_k of (3.1) according to:

$$\forall x \in \Omega_k,\ v_k(x) = \begin{cases} u_k(x) & \text{if } u_k(x) \cap \mathcal{T}_S = \emptyset \\ y - x & \text{if } u_k(x) \cap \mathcal{T}_S = \{y\} \end{cases} \tag{3.3}$$

Doing so, at each step k the intersection between the vector $u_k(x)$ and the triangulation $\mathcal{T}_S$ is checked for all x vertex of Γ_k^D. In case of multiples intersection points, the point y closest to x is retained. At each step k, the boundaries Γ_k^D and Γ_k^N are allowed to vary according to the previous ray/surface intersection test: if an intersection point y is found, then x is clamped at this point, so that $\Gamma_{k+1}^D = \Gamma_k^D \cup \{y\}$ and $\Gamma_{k+1}^N = \Gamma_k^N \setminus \{y\}$.

Doing so, points on Ω_k are advected according to equation (3.1) until they intercept the triangulation $\mathcal{T}_S$. Whenever a contact between the advecting shape and the source triangulation occurs, the first is clamped and forced to not cross the boundary of the latter. The advecting sequence of boundaries gets closer and closer to the source mesh $\mathcal{T}_S$ thanks to the strict inequality:

$$d_H(\Gamma_{k+1}, \mathcal{T}_S) < d_H(\Gamma_k, \mathcal{T}_S),$$

where $d_H(\cdot, \cdot)$ is the Hausdorff distance between the two triangulations. Indeed, for k sufficiently large the advecting surface Γ_k defines a closed boundary which wraps the source triangulation $\mathcal{T}_S$.

3.2 Numerical issues

As far as the numerical setting is concerned, the template shape Ω_0 is discretized as a volumetric mesh $\mathcal{T}_0$, e.g. filled with tetrahedra. The triangulation $\mathcal{S}_0$ obtained by taking the internal boundary triangles of $\mathcal{T}_0$ supplies a simplicial mesh of the boundary Γ_0 of Ω_0. From the numerical point of view, the existence of a common subset ω between $\mathcal{S}_0$ and $\mathcal{T}_S$ corresponds to a global alignment and

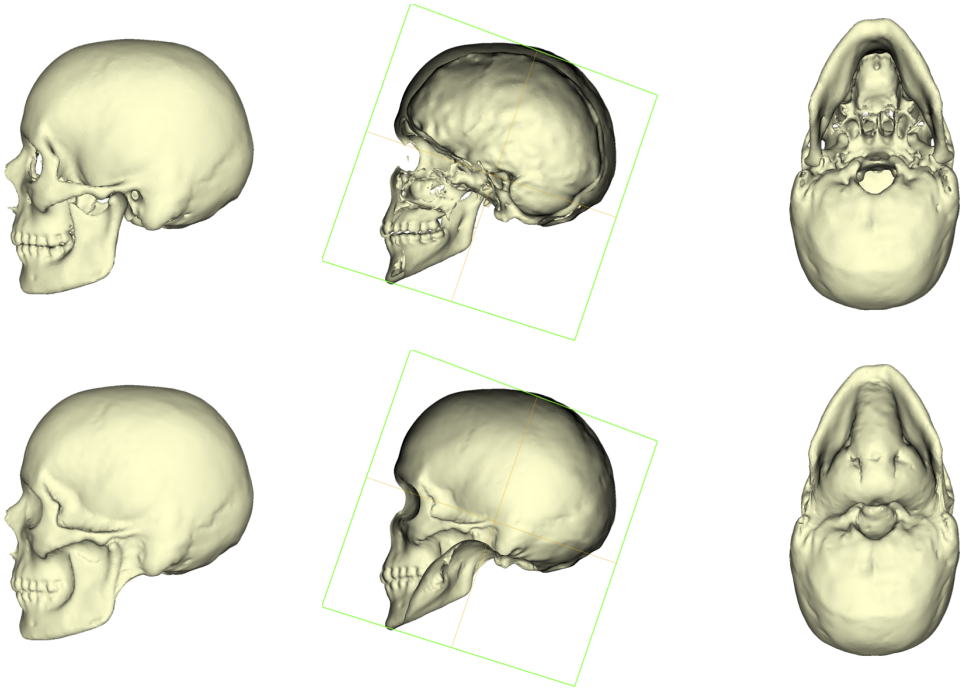

Figure 7 – Top: 3d model of the skull. Bottom: wrapped skull.

scaling of the two meshes. Starting from the template mesh $\mathcal{T}_0$, we perform an iterative algorithm in order to get a sequence $(\mathcal{T}_k, \mathcal{S}_k)$ of meshes with decreasing values of $d_H(\mathcal{S}_k, \mathcal{T}_S)$.

Given a fixed integer N, the procedure ends whenever the set Γ_k^D is empty (all the points in $\mathcal{S}_k$ have reached $\mathcal{T}_S$) or if N iterations of the process occur without registering a new ray/triangle intersection. The last condition deals with the potential presence of holes in $\mathcal{T}_S$.

At each iteration the solution u_k of the elastic system (3.1) related to the domain $\Omega = \mathcal{T}_k$ with $\Gamma^D = \mathcal{S}_k^D$ and $\Gamma^N = \mathcal{S}_k^N$ is computed by the Finite Elements Method. Figures 6 and 7 depict the wrapping of a skull triangulation. The parameters we used for assembling the elastic system (3.1) are

$$\lambda = \frac{E\nu}{(1+\nu)(1-2\nu)} \quad \text{and} \quad \mu = \frac{E}{2(1+\nu)},$$

where $E = 10000\ kPa$ is the Young modulus and $\nu = 0.1$ is the Poisson coefficient, which corresponds to a very soft and compressible material and the pression is $p = 200\ kPa$. The procedure ends after 35 iterations with $N = 5$, running in a few minutes on a standard laptop computer. About 85% of points on the triangulation $\mathcal{S}_{35}$ are clamped on the surface mesh $\mathcal{T}_S$.

4 Inter-subject shape matching

Shape morphing or matching arises in a wide variety of situations in areas from biomedical engineering to computer graphics and scientific computing. Beyond the specific stakes to each particular application, the general issue is to find one transformation from a given 'template' shape Ω_0 into a 'target' Ω_T (see Figure 8). Such a transformation may be used as a means to appraise how much Ω_0 and Ω_T differ from one another - for instance in shape retrieval, classification or recognition - or to achieve physically the transformation from Ω_0 to Ω_T (in shape registration, reconstruction,

or shape simplification). See for instance [41] and references therein for an overview of several related applications. In the facial reconstruction context, shape matching may be a key ingredient for studying the shape database, making possible the generation of average shapes -eventually weighted according to their 'similarity'- as well as for driving the registration of the craniofacial template onto the unknown skull.

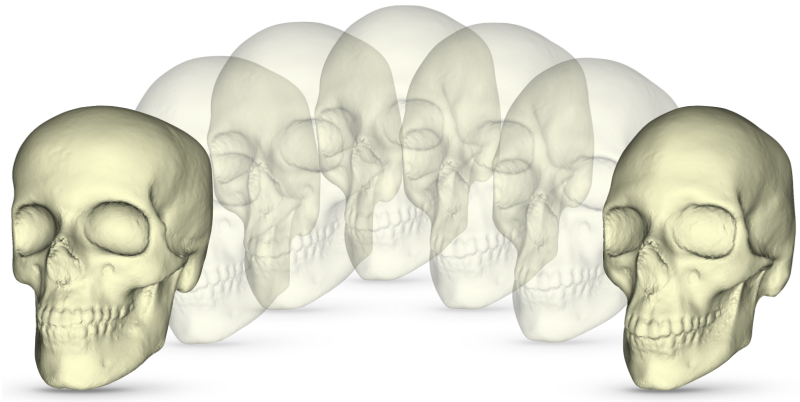

Figure 8 – Elastic shape morphing allowing to deform a template onto another.

Understandably enough, a great deal of work has been devoted to shape matching, and we limit ourselves to mentioning a few approaches. In [5], the authors start by distributing sample points on the contour of both shapes, that will be matched according to their 'shape context'. They eventually infer a global transformation from this point-to-point correspondance. In the field of computational anatomy, a series of articles, [4, 17, 21] among others, have suggested to describe a sought diffeomorphism between Ω_0 and Ω_T as the flow of a velocity field v, and to cast the search for v as an optimal control problem. More recently, in the field of Computer Graphics, the optimal transport point of view has been used to displace an input tetrahedral mesh onto a given object [28].

Our problem is stated as follows: given a 'template' shape Ω_0, numerically described by means of a (conforming) computational mesh, and a 'target' shape Ω_T, we aim at deforming (iteratively) the mesh of Ω_0 into a computational mesh of Ω_T. Such a technique could be applied, for instance, to the reconstruction of a computational mesh Ω_T from invalid data, to transport quantities of interest from Ω_0 to Ω_T, etc. To achieve our purpose, we rely on a method which has much in common with that of [2], borrowing techniques from shape optimization, and more generally optimal control. Under the assumption that Ω_0 and Ω_T share the same topology, the desired transformation from Ω_0 to Ω_T is realized as a sequence of elastic displacements, which are obtained by minimizing an energy functional based on the distance between Ω_0 and Ω_T. In doing so, it is expected that the deformation will be easier to achieve in numerical practice, and in particular by limiting the troubles due to mesh tangling. In this section, we briefly present the mathematical framework and some numerical issues related to the method. We refer to [7] for more details and for 2d and 3d numerical examples.

4.1 Presentation of the method

The discrepancy between a reference shape Ω and a target shape Ω_T is measured by the following functional $J(\Omega)$ of the domain:

$$J(\Omega) = \int_\Omega d_{\Omega_T}(x)dx, \tag{4.1}$$

which involves the Euclidean *signed distance function* d_{Ω_T} to Ω_T, defined as:

$$\forall x \in \mathbb{R}^d,\ \ d_{\Omega_T}(x) = \begin{cases} -d(x, \partial\Omega_T) & \text{if } x \in \Omega_T, \\ 0 & \text{if } x \in \partial\Omega_T, \\ d(x, \partial\Omega_T) & \text{if } x \in {}^c\overline{\Omega_T}. \end{cases}$$

In the above formula, $d(\cdot, \partial\Omega_T)$ denotes the usual Euclidean distance function to $\partial\Omega_T$.

In order to decrease the value of $J(\Omega)$, the domain Ω must expand in the regions of the ambient space $\mathbb{R}^3$ where d_{Ω_T} is negative (that is, in the regions comprised in Ω_T), and to retract in those where it is positive. Note that the functional $J(\Omega)$ has a unique, global minimizer $\Omega = \Omega_T$, and no extra local minimum point provided Ω_T is connected. It is then expected that an iterative (e.g. gradient-based) algorithm for minimizing $J(\Omega)$, starting from Ω_0, will lead to an interesting way to transform Ω_0 into Ω_T. This paves the way for an iterative algorithm, producing a sequence $(\Omega_k)_{k=0,\dots}$ of shapes, which are 'closer and closer' to Ω_T: at each step, Ω_k is updated according to

$$\Omega_{k+1} = (I + u)(\Omega_k), \tag{4.2}$$

where u is a suitable descent direction for $J(\Omega)$. Now, imagine that all the considered shapes Ω are filled with a linear elastic material. We can compute the unique solution u of the elasticity equations (3.1) where the pression p is taken equal to $-d_{\Omega_T}$. This vector field u is naturally a descent direction for $J(\Omega)$ since by a classical calculation (see [7] for more details), the shape derivative of the function $J(\Omega)$ satisfies

$$J'(\Omega)(u) \leq 0.$$

4.2 Numerical issues

As far as the numerical setting is concerned, the template shape Ω_0 is discretized as a simplicial mesh (i.e. a triangulation), and the target shape Ω_T is supplied through its signed distance function, e.g. as a piecewise affine function on the fixed mesh $\mathcal{T}_D$ of a large computational domain D.

Starting from the template shape Ω_0 we perform a gradient descent algorithm with adaptive step size in order to get a sequence of pairs $(\Omega_k,\ \mathcal{T}_k)$ of domains and their corresponding meshes with decreasing values of $J(\Omega_k)$. The algorithm stops when the step size is smaller than a fixed tolerance ε.

Remark 4.1. *1. The only information required about the target shape Ω_T is the datum of its signed distance function which can be defined on a possibly non-conforming mesh (e.g. showing small gaps, overlapping entities, etc.). Such an implicitly-defined domains can be explicitly meshed into a valid configuration following the approach described in [15]. See Figure 11 for an example of such a procedure.*

2. The global mapping from Ω_0 to Ω_T is easily recovered by the composition of the different displacements between each iteration.

3. The computational meshes used to perform the calculation are non uniform; they are refined in the vicinity of the boundaries according to a curvature based sizing function and coarsened in the interior of the domain. This has proven to prevent severe distorsion/tangling of the elements (avoiding the need to remesh the domain) and hence to increase the efficiency of the overall algorithm.

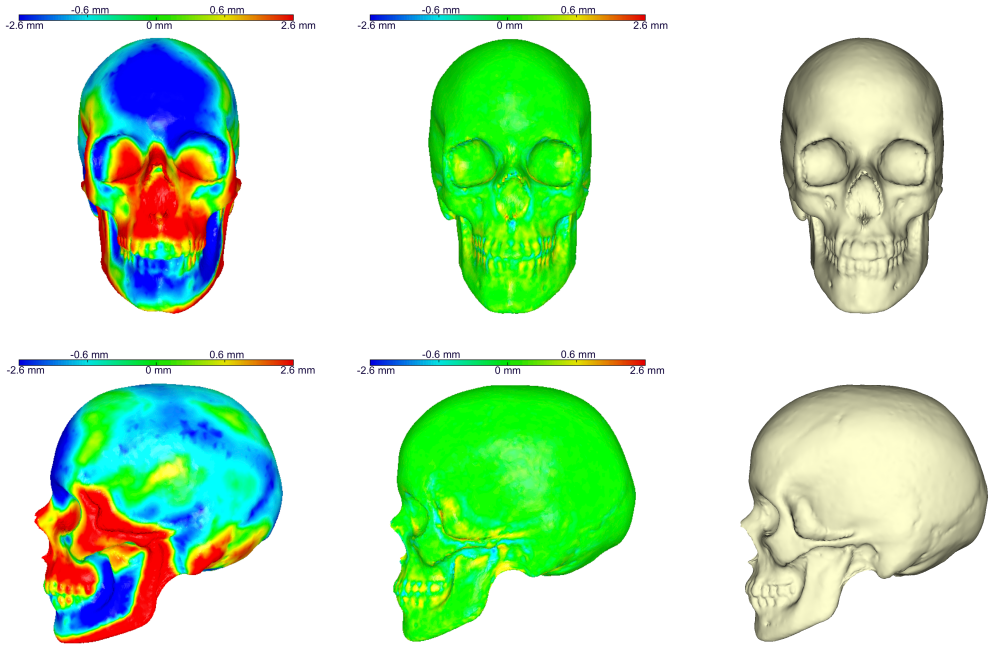

(a) (b) (c)

Figure 9 – (a) Template shape Ω_0 and discrepancy w.r.t. the target shape. (b) Deformed shape Ω_k for $k = 300$ and discrepancy w.r.t. the target shape. (c) Target shape. (For interpretation of the references to color in this figure legend, the reader is referred to the web version of the article.)

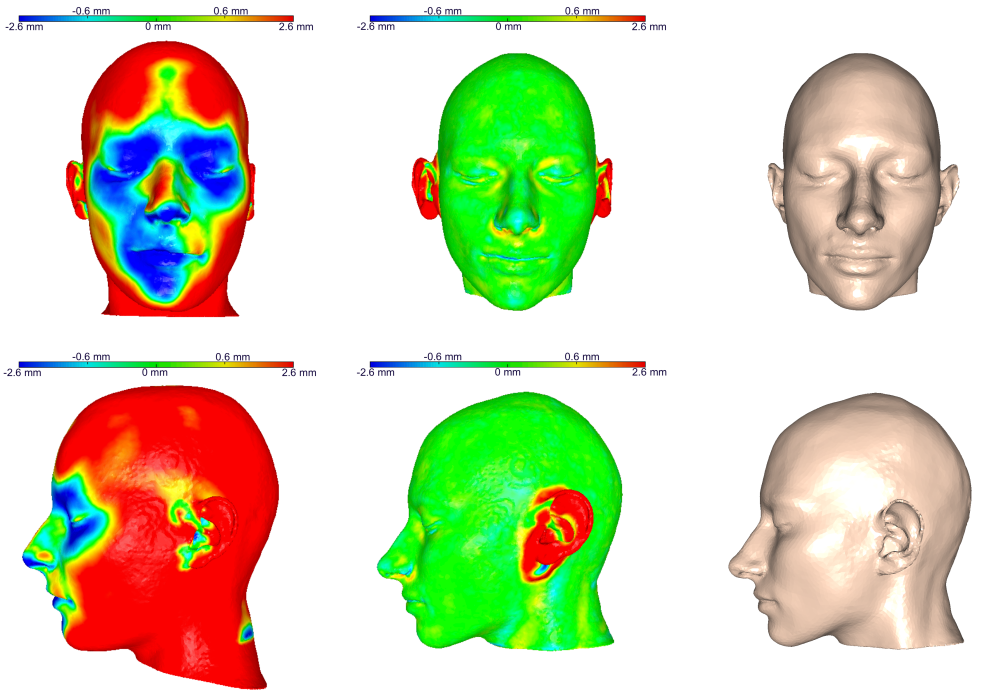

(a) (b) (c)

Figure 10 – : (a) Template shape Ω_0 and discrepancy w.r.t. the target shape. (b) Deformed shape Ω_k for $k = 400$ and discrepancy w.r.t. the target shape. (c) Target shape. (For interpretation of the references to color in this figure legend, the reader is referred to the web version of the article.)

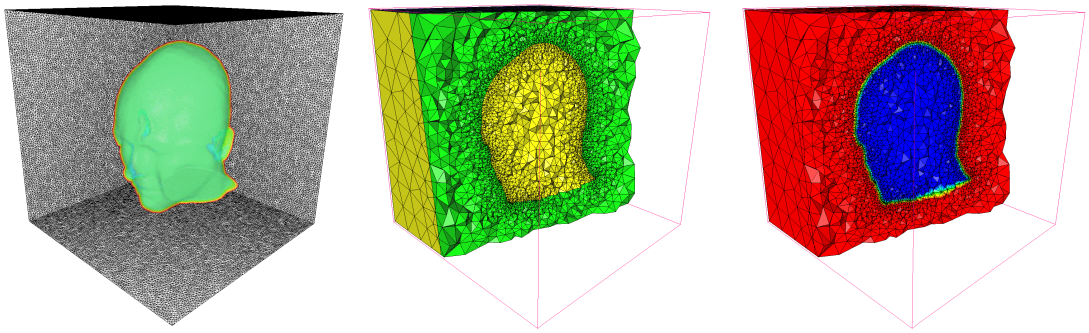

(a) (b) (c)

Figure 11 – (a) Target shape Ω_T as the zero level set of the signed distance function; (b) Adaptative remeshing of the computational box; (c) Color map displaying the signed distance function to the target shape.

In the proposed examples, the calculation of the signed distance function to Ω_T is performed using the algorithm described in [14]. At first, Figure 9 depicts the matching of two skull shapes. The template mesh $\mathcal{T}_0$ has about 130 000 surface triangles, and the convergence of the gradient descent procedure is obtained in 300 iterations for a given tolerance $\varepsilon = 10^{-6}$. The L^2 norm of the distance d_{Ω_T} calculated on the boundary of the resulting shape Ω_{300} equals 0.1 mm (much smaller than the minimal mesh size), revealing an excellent matching of Ω_T.

Next, we consider a face example; see Figure 10. The template mesh $\mathcal{T}_0$ has about 90 000 triangles, and 400 iterations of the gradient descent algorithm have been performed to achieve convergence for a tolerance $\varepsilon = 10^{-6}$, running in a few minutes on a standard laptop computer. The L^2 norm of the distance d_{Ω_T} calculated on the boundary of the final shape Ω_{400} is 0.2 mm (again, much smaller than the minimal mesh size).

Remark 4.2. *We decided to not include the ears in the face matching process, since these structures are not linked with the underlying skull morphology. This procedure is simply done by defining patches on the face template and including in the minimization of $J(\Omega)$ only the interesting patches.*

5 Registration of the craniofacial template onto the unknown skull

The parametrization of skull, face and soft tissue information depends strongly on the nature of the database. Using CT scans of living subjects allows a dense representation of the craniofacial information. If closed surface models of both skull and face are available, then the craniofacial template may be described in terms of the 3d domain delimitated by the outer face and the inner skull boundaries, generating a 3d 'mask' which incorporates the soft tissue information. A single craniofacial template may be used for producing templates of all individual in the database. The procedure relies on the shape matching technique (see Section 4), generating a set of vector fields, one for each individual, each of them allowing to deform the template shape onto a specific shape of the database. Doing so, our method is able to generate valid computational meshes of all the shapes in the database. Moreover, dense intra-subject correspondences are naturally established, allowing the generation of a continuum spectrum of faces issued from the (convex) combination of

the individuals in the database.

Various mathematical methods have been proposed for deforming the craniofacial template onto the unknown skull, as volume distortion functions, radial basis function [35], or PCA. Our method reposes on the 'physical' deformation of the craniofacial template onto the unknown skull. The mask is deformed according to a displacement field prescribed on the skull boundary, measuring the deformation of the skull template into the unknown skull. Under the effect of boundary changes, the mask is allowed to deform as a linear elastic material, resulting in a deformed face shape which is now adapted to the unknown skull. The use of elasticity for soft tissue deformation is largely customized in the field of computational maxillofacial surgery [8, 43].

5.1 Craniofacial templates generation

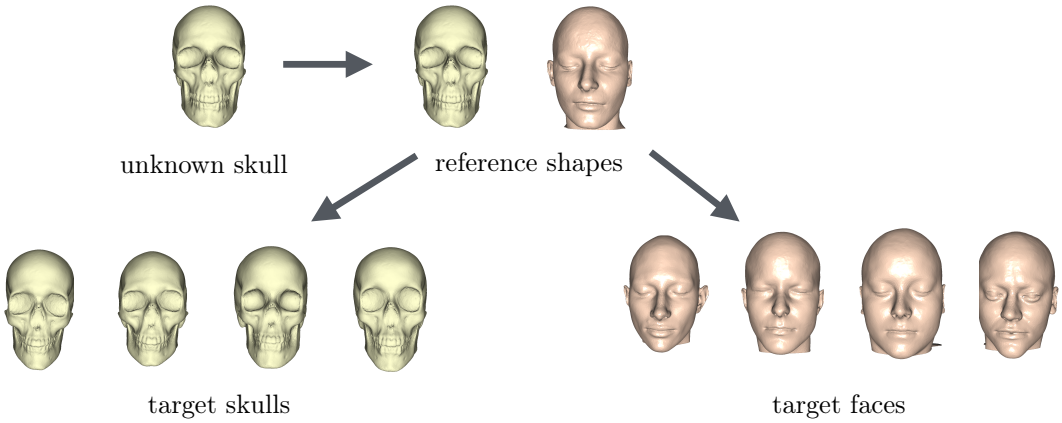

Figure 12 – Matching skull and face templates within the database

The optimization algorithm described in the previous section was used to match all the shapes among the database. The shapes are initially roughly aligned by an Iterative Closest Point algorithm. Let $\{S_i\}_{i=0,\cdots,N}$ and $\{F_i\}_{i=0,\cdots,N}$ be the collection of respectively skull and face shapes. A reference template shape, say S_0, is chosen inside the database and matched onto all the $S_1, \cdots, S_N$ skulls (with global displacements $u_1, \cdots, u_N$). The reference face F_0 (coupled with S_0) is matched onto all the $F_1, \cdots, F_N$ faces (with global displacements $v_1, \cdots, v_N$). In order to do so, computational meshes of the reference shapes are generated, to ensure convergence of the finite elements simulation. The original geometrical meshes are remeshed by controlling elements shape quality and mesh gradation (the size variation between neighboring triangles). All the other shapes in the database are now implicitly supplied through the signed distance function. Thanks to the matching process, we are able to describe all the shapes in the database in terms of two computational meshes (reference skull and face) and a set of displacement fields. Each shape is defined by he mapping:

$$S_i = (I + u_i)(S_0) \quad \forall i = 1, \cdots, N \qquad F_i = (I + v_i)(F_0) \quad \forall i = 1, \cdots, N.$$

Note that at this step all the meshes share the same number of elements (vertices, triangles) and the same connectivity. Doing so, the computation of average shapes turns into trivial average of

the vector fields. Any convex combination w of the form:

$$w = \sum_{i=1}^{N} \alpha_i v_i, \qquad \text{with } \alpha_i \in \mathbb{R}, \alpha_i \in [0,1], \sum_i \alpha_i = 1,$$

defines a new shape W through the mapping:

$$W = (I + w)(\mathcal{F}_0).$$

See Figure 13 for an exemple of generation of new shapes as a convex combination of three templates.

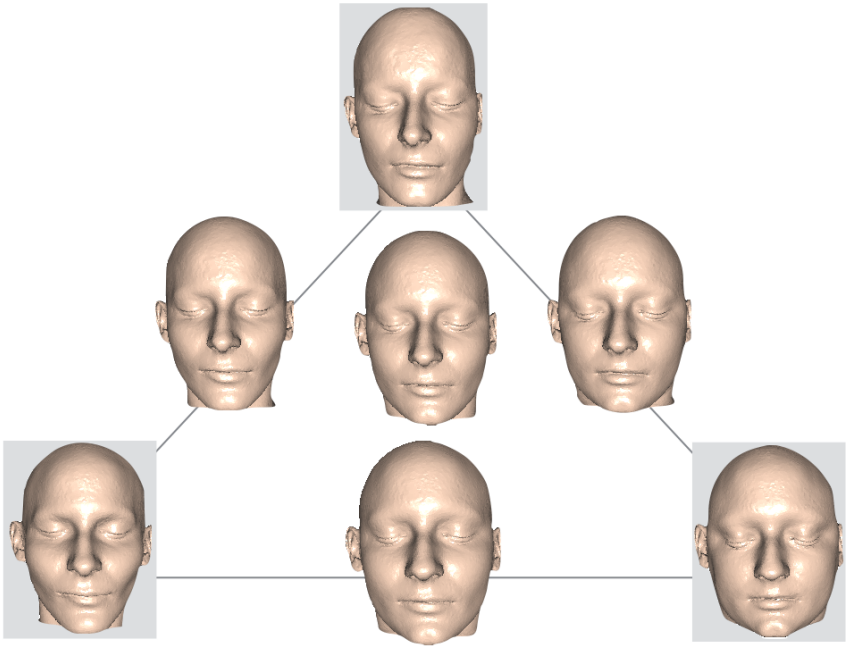

Figure 13 – The corners of the triangle display three face templates. The top template is chosen as reference shape and matched into the bottom right template and the bottom left template. The middle of the triangle and the mid-edges display the 'barycenter' faces computed by averaging the displacement fields.

5.2 Face-to-skull mapping via skull matching

The link between the unknown skull S_T and the database skulls is given by the mapping:

$$S_T = \big(I + u_0\big)\big(I + u_i\big)^{-1}(S_i) \quad \forall i = 1, \cdots, N \tag{5.1}$$

where u_0 is the global displacement mapping the reference skull S_0 onto the target skull S_T and $\{u_i\}_{i=0,\cdots,N}$ are the pre-calculated displacements mapping the reference skull S_0 onto the target skull templates $\{S_i\}_{i=0,\cdots,N}$ (see Figure 12). The mapping (5.1) will now drive the deformation of the face templates.

The link between the unknown skull S_T and the template F_i is inferred by the following procedure:

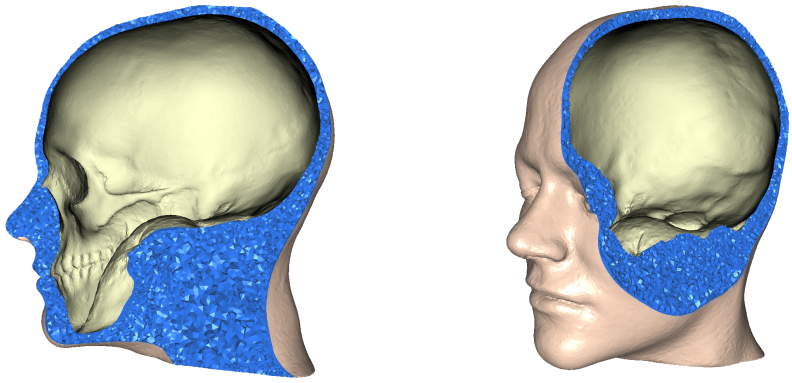

Figure 14 – Generation of a 3d craniofacial template encoding soft tissue information.

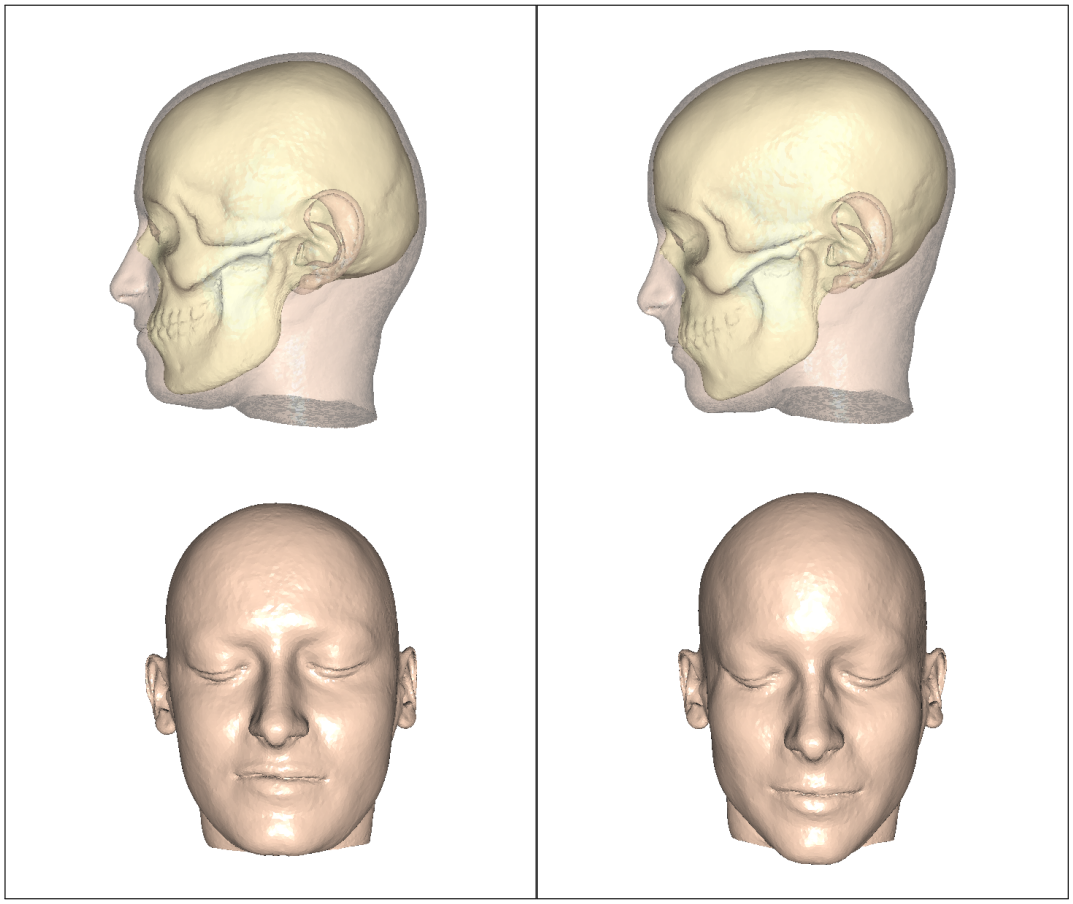

(a) Initial (b) Final

Figure 15 – Elastic deformation of the craniofacial template under the effect of skull changes.

1. the volume between the coupled surfaces $\{(S_i, F_i)\}_{i=0,\cdots,N}$ is filled with an elastic material, generating N 3d masks $\{M_i\}_{i=0,\cdots,N}$(see Figure 14);

2. the skull S_i is mapped onto the unknown skull S_T and the 3d mask is elastically deformed under the effect of the boundary changes (see Figure 15). The deformation of the template M_i is achieved as the solution U_i of an elastic problem similar to (3.1), in which we impose non homogeneous displacement condition $U_i = u_i$ on the skull boundary and zero traction conditions on the outer boundary.

The soft tissue deformation step produces N new faces, each of one obtained by linking a specific craniofacial template with the unknown skull. These facial items (all or a small subset) are then combined together -for example by building a statistical shape model- to predict the most plausible face associated to the unknown skull.

6 Results and discussion

The validation of a method for facial reconstruction is of tremendous importance for the purpose of legitimating its use during a criminal investigation. The natural way to address this problem is the "leave-one-out scheme". One individual is removed from the database and the method is employed to reconstruct his face given the sole skull. Then the predicted shape is compared with the available "unknown face". The discrepancy between the two shapes can be evaluated mathematically by computing distances (Euclidean, Hausdorff, Gromov-Hausdorff or Wasserstein) between them. However, since the final purpose of the method is a positive identification, a *recognition* test can be also employed for revealing the power of prediction of the method [11]. A recognition test consist in showing the predicted face together with a sample of faces which contains the unknown face. Then the human volunteer indicates the face (or faces) which is (are) closer to the predicted one. The positive outcome will then correspond to the identification of the unknown face among the sample. Such a study for the method proposed in this article is under process and results will be published in a forthcoming paper.

Here we limit ourselves in presenting an example of reconstruction in one test case. According with the leave-one-out scheme, one individual is removed from the database and a prediction of his face is generated by deforming all the database templates onto his skull (unknown skull). Figure 16 shows the average shape obtained by computing the geometric mean of all the faces transported onto the unknown skull. The discrepancy $\mathcal{D}$ between a surface Γ and a reference surface Γ_0 is evaluated by the following mean error:

$$\mathcal{D}(\Gamma, \Gamma_0) = \left(\frac{1}{|\Gamma|} \int_\Gamma d^2(x, \Gamma_0) dx \right)^{\frac{1}{2}},$$

where $|\Gamma|$ is the measure of Γ and $d(\cdot, \Gamma_0)$ is the Euclidean distance to Γ_0. This error estimator is used for evaluating the vicinity between:

1. the skull templates of the database and the unknown skull;

2. the face templates of the database and the unknown face associated with the unknown skull;

3. the face templates after deformation onto the unknown skull and the unknown face associated with the unknown skull;

4. the face templates of the database and the reconstructed average face.

The minimal, maximum and mean values of $\mathcal{D}$ for the 25 templates of the database are reported in Table 1. In particular, we observe that the discrepancy between the face template and the unknown

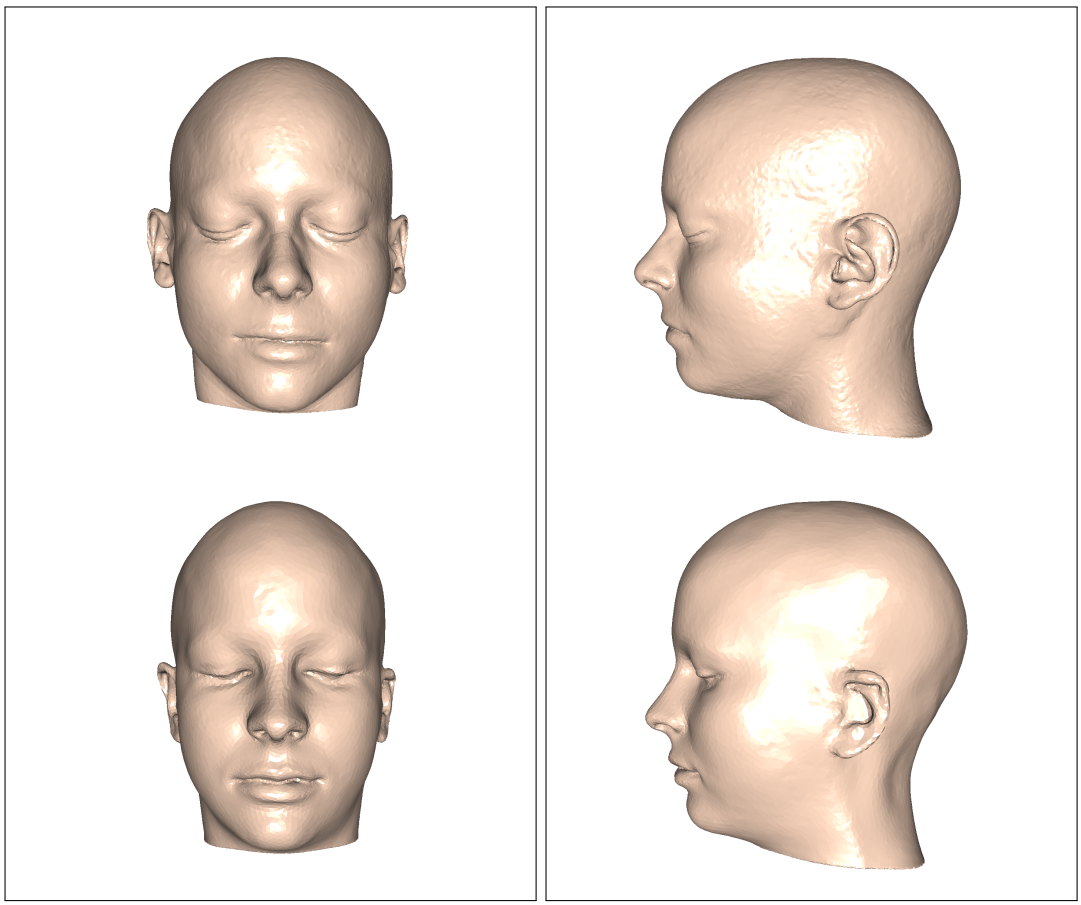

(a) Front view (b) Side view

Figure 16 – Top row: predicted face obtained as the geometric mean of all the face templates deformed onto the unknown skull. Bottom row: unknown face.

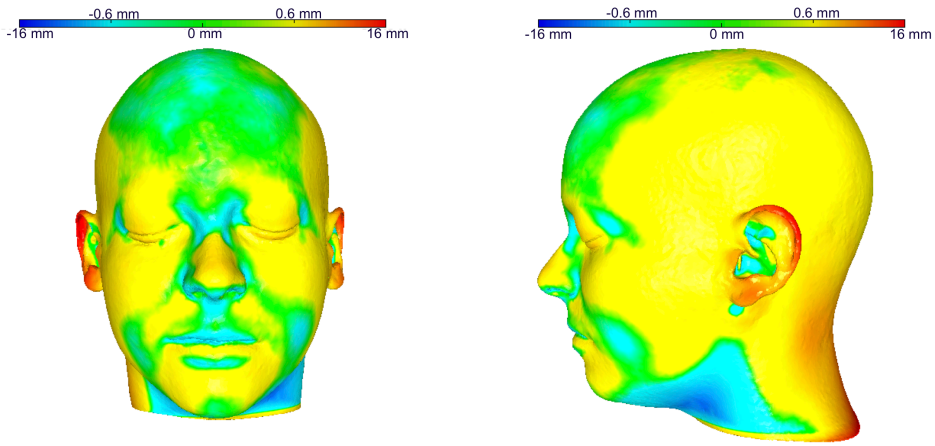

Figure 17 – Discrepancy between the predicted face obtained as the geometric mean of all the face templates deformed onto the unknown skull and the unknown face.(For interpretation of the references to color in this figure legend, the reader is referred to the web version of the article.)

face is smaller after deformation for all the individuals. Thus, the elastic transformation used in the method seems to be a good tool to transport the faces close to the unknown face. Moreover, our a posteriori error computation highlights the fact that the face showing after deformation the smallest discrepancy w.r.t. the unknown face (2.93 mm) corresponds to the skull showing the smallest discrepancy w.r.t. the unknown skull (5.44 mm). Finally, the discrepancy between the unknown face and the average predicted face is 4.24 mm. Is is smaller than the discrepancy for any individual in the database, so this measure $\mathcal{D}$ can be used for an automatic numerical identification. Figure 17 shows the distribution of the error over the surface for the reconstruction. We remark that in the regions of interest (excluding ears and neck in particular), the error is less than a millimeter. We also remark that in these regions we overestimate the thickness of the tissue. Using the information coming from the BMI of the individuals in the database could be a way to propose different reconstructed faces corresponding to different BMI of the unknown individual.

Discrepancy between $\cdots$	min	mean	max
1. skulls of the database and the unknown skull	5.44 mm	7.86 mm	13.46 mm
2. faces of the database and the unknown face	5.02 mm	8.94 mm	15.69 mm
3. faces after deformation and the unknown face	2.93 mm	5.8 mm	10.35 mm
4. faces of the database and the average predicted face	4.54 mm	7.03 mm	11.28 mm

Table 1 – Discrepancy between shapes for our test case.

7 Conclusion

The proposed reconstruction method reposes on the 'physical' deformation of templates of coupled faces and skulls onto the unknown target skull. In practice, the acquisition of full head scans of healthy subjects is still a difficult process. Most of the time one can access to clinical data, meaning that the patients present anomalies of the morphology or that the scans are only partial (in the case of maxillo-facial examination for surgery purposes). The access to an adequate database of full heads of healthy subjects would improve enormously the final product of our method. Even if our experiments were carried out on a small collection of 26 individuals, our method produced promising results. The proposed method for shape matching allows an accurate registration. The method is simple to implement and doesn't need any a prior landmarks correspondence.

Aknowledgements

The authors would like to kindly thank F. Tilotta, Y. Rozenholc and J. Glaunes for providing the CT head data [38], L. Uro and S. Slimani for segmenting part of the DICOM images, P. Frey, M. Friess and P. Deuflhard, whose comments improved the quality of the manuscript, Loic Norgeot, C. Dapogny, the ISCD team and the partners of project FaciLe for fruitful meetings and D. Baum, S. Zachow and the ZIB team for interesting discussions.

References

[1] G. Allaire, *Conception optimale de structures*, Mathématiques & Applications, **58**, Springer Verlag, Heidelberg (2006).

[2] R. Bajcsy and S. Kovacic *Multiresolution elastic matching*, Computer Vision, Graphics and Image Processing, 46, (1989) pp. 1–21.

[3] T. J. Baker, *Mesh Movement and Metamorphosis*, Eng. Comput. 18, 1, (2002), pp. 188–198.

[4] M.F. Beg, M.I. Miller, A. Trouvé L. Younes, *Computing large deformation metric mappings via geodesic flows of diffeomorphisms*, Int. J. Comput. Vis., 61, (2005), pp. 139–157.

[5] S. Belongie, J. Malik, J. Puzicha, *Shape matching and object recognition using shape contexts*, IEEE Transactions on Pattern Analysis and Machine Intelligence, 24 (4), (2002), pp. 509–522..

[6] J. Céa, *Conception optimale ou identification de formes, calcul rapide de la dérivée directionnelle de la fonction coût*, Math. Model. Num. 20, 3 (1986), pp. 371–420.

[7] M. de Buhan, C. Dapogny, P. Frey C. Nardoni, *An optimization method for shape matching*, C. R. Acad. Sci. Paris; Ser. I 354 (2016), pp. 783-787.

[8] M. Chabanas, Vincent Luboz Yohan Payan, *Patient specific finite element model of the face soft tissues for computer-assisted maxillofacial surgery*, Med Image Anal. 2003 Jun;7(2):131-51.

[9] P.G. Ciarlet, *Mathematical Elasticity, vol I: Three Dimensional Elasticity*, North Holland Publishing Company (1988).

[10] P. Claes, *A robust statistical surface registration framework using implicit function representations: appication in craniofacial reconstruction*, doctoral thesis, 2007.

[11] P. Claes, D. Vandermeulen, S. De Greef, G. Willems, J.G. Clement P. Suetens, *Computerized craniofacial reconstruction: Conceptual framework and review*, Forensic Science International (2010).

[12] P. Claes, D. Vandermeulen, S. De Greef, G. Willems, J.G. Clement P. Suetens, *Craniofacial reconstruction using a combined statistical model of face shape and soft tissue depths: Methodology and validation*, Forensic Science International (2006).

[13] A. Claisse P. Frey, *A nonlinear PDE model for reconstructing a regular surface from sampled data using a level set formulation on triangular meshes*, Journal of Computational Physics, Volume 230, Issue 12, pp 4636-4656 (2011).

[14] C. Dapogny P. Frey, *Computation of the signed distance function to a discrete contour on adapted triangulation*, Calcolo, Volume 49, Issue 3, pp. 193-219 (2012).

[15] C. Dapogny, C. Dobrzynski P. Frey, *Three-dimensional adaptive domain remeshing, implicit domain meshing, and applications to free and moving boundary problems*, J. Comput. Phys, 262, pp 358–378 (2014).

[16] Y. Duan, L.Yang, H. Qin D. Samaras, *Shape Reconstruction from 3D and 2D Data Using PDE-Based Deformable Surfaces*, European Conference on Computer Vision pp. 238-251 (2004).

[17] P. Dupuis, U. Grenander, M.I. Miller, *Variational problems on flows of diffeomorphisms for image matching*, Q. Appl. Math., 56, (1998), pp. 587–600.

[18] P. Frey, *Generation and adaptation of computational surface meshes from discrete anatomical data*, Int. J. Numer. Meth. Engng, 60:1049-1074 (2004).

[19] F. de Gournay, *Velocity extension for the level-set method and multiple eigenvalues in shape optimization.* SIAM J. on Control and Optim., 45, no. 1, 343–367 (2006).

[20] S. De Greef, P. Claes, D. Vandermeulen, W. Mollemans, P. Suetens G. Willems, *Large-scale in-vivo Caucasian facial soft tissue thickness database for craniofacial reconstruction*, Forensic Science International (2006).

[21] U. Grenander M.I. Miller, *Computational anatomy: an emerging discipline*, Current and future challenges in the applications of mathematics (Providence, RI, 1997), Quart. Appl. Math. 56, no. 4, (1998), pp. 617–694.

[22] C. M. Grewe, L. Schreiber S. Zachow, *Fast and Accurate Digital Morphometry of Facial Expressions*, Facial Plastic Surgery, 2015.

[23] A. Henrot M. Pierre, *Variation et optimisation de formes, une analyse géométrique*, Mathématiques et Applications 48, Springer, Heidelberg, (2005).

[24] H.S. Hwang, M.K. Park, W.J. Lee, J.H. Cho, B.K. Kim, C. Wilkinson,, *Facial Soft Tissue Thickness Database for Craniofacial Reconstruction in Korean Adults*, Journal of Forensic Science (2012).

[25] M. W. Jones, *Facial Reconstruction Using Volumetric Data*, International Vision Modeling and Visualisation Conference, Stuttgart (2003).

[26] K. Kahler, J. Haber H.P. Seidel, *Reanimating the Dead: Reconstruction of Expressive Faces from Skull Data*, ACM Transactions on Graphics, 22, pp. 554-561 (2003).

[27] A. Kustár, L. Forró, I. Kalina, F. Fazekas, S. Honti, S. Makra M. Friess, *FACE R A 3D Database of 400 Living Individuals Full Head CT and Face Scans and Preliminary GMM Analysis for Craniofacial Reconstruction*, Journal of Forensic Science, 2013.

[28] B. Lévy, *A numerical algorithm for L_2 semi-discrete optimal transport in 3D*, ESAIM: Math. Model. Numer. Anal., 49, 6, (2015), pp. 1693–1715.

[29] J. Miller, D. Breen, W. Lorensen, R. O'Bara, M. Wozny, Geometrically Deformed Models: A Method for Extracting Closed Geometric Models Form Volume Data, SIGGRAPH '91 Proceedings of the 18th annual conference on Computer graphics and interactive techniques, pp. 217-226, (1991).

[30] S. Miyasaka, M. Yoshinoa, K. Imaizumia S. Seta, *The computer-aided facial reconstruction system*, Forensic Science International (1995).

[31] F. Murat J. Simon, *Sur le contrôle par un domaine géométrique*, Technical Report RR-76015, Laboratoire d'Analyse Numérique (1976).

[32] P. Paysan, M. L'uthi, T. Albrecht, A. Lerch, B. Amberg, F. Santini T. Vetter, *Face reconstruction from skull shapes and physical attributes*, Lecture Notes in Computer Science, Pattern Recognition, Springer, Berlin/Heidelberg, 2009 ,pp. 232-241.

[33] J. Prag R. Neave, *Making Faces: Using Forensic and Archaeological Evidence*, The Trustees of the British Museum, 1997.

[34] L.A. Nelson S.D. Michael, *The application of volume deformation to three dimensional facial reconstruction: A comparison with previous techniques*, Forensic Science International (1998).

[35] G. Quatrehomme, S. Cotin, G. Subsol, H. Delingette, Y. Garidel, G. Grévin, M. Fidrich, P. Bailet A. Ollier, *A Fully Three-Dimensional Method for Facial Reconstruction Based on Deformable Models*, Journal of Forensic Science, 1997.

[36] L. J. Short, B. Khambay, A. Ayoub, C. Erolin, C. Rynn C. Wilkinson, *Validation of a computer modelled forensic facial reconstruction technique using CT data from live subjects: A pilot study*, Forensic Science International (2014).

[37] D. Stalling, M. Westerhoff H.C. Hege, *Amira: a Highly Interactive System for Visual Data Analysis*, In: Charles D. Hansen and Chris R. Johnson (eds.), The Visualization Handbook, pp. 749-767, Elsevier, 2005.

[38] F. M. Tilotta, F. J. P. Richard, J. A. Glaunès, M. Berar, S. Gey, S. Verdille, Y. Rozenholc J.F. Gaudy, *Construction and analysis of a head CT-scan database for craniofacial reconstruction*, Forensic Science International, 2009, 191 (1-3), pp.112.e1-112.e12.

[39] F. M. Tilotta, J. A. Glaunès, F. J. P. Richard Y. Rozenholc, *A local technique based on vectorized surfaces for craniofacial reconstruction*, Forensic Science International 2010, 200 (1-3), pp.50-59.

[40] D. Vandermulen, P. Claes, D. Loeckx, S. De Greef, G. Willems Suetens, *Computerized craniofacial reconstruction using CT-derived implicit surface representations*, Forensic Science International, 2006.

[41] R.C. Veltkamp, *Shape matching: Similarity measures and algorithms*, In Shape Modeling and Applications, SMI 2001, IEEE, (2001), pp. 188–197.

[42] C. Wilkinson, *Computerized forensic facial reconstruction A review of current systems*, Forensic Science, Medicine, and Pathology , 2005, Volume 1, Issue 3, pp 173–177.

[43] S. Zachow, E.Gladiline, H.-C. Hege P. Deuflhard, *Finite-Element Simulation for Soft Tissue Prediction*, In: Lemke, H.U. et al (eds.): Computer Assisted Radiology and Surgery (CARS), Elsevier Science B.V., pp. 23-28 (2000).